Automated quantitative analysis of rheumatoid arthritis lesions in MRI

K. K. Leung[1], M. Holden[2], N. Saeed[3], K. J. Brooks[3], J. B. Buckton[4], A. Williams[5], S. P. Campbell[3], K. Changani[3], D. G. Reid[3], D. Rueckert[6], J. V. Hajnal[7], D. L. Hill[1]

[1]Department of Image Sciences, King's College London, London, United Kingdom, [2]BioMedIA Lab, CSIRO-ICT, Sydney, New South Wales, Australia, [3]Imaging Centre, ri-CEDD, GlaxoSmithKline, Welwyn, United Kingdom, [4]RA Disease Biology, ri-CEDD, GlaxoSmithKline, Welwyn, United Kingdom, [5]Pathology, Safety Assessment, GlaxoSmithKline, Welwyn, United Kingdom, [6]Department of Computing, Imperial College, London, United Kingdom, [7]Imaging Sciences Department, Imperial College, London, United Kingdom

Introduction:

Rheumatoid arthritis (RA) is a chronic, autoimmune, inflammatory joint disease which, until recently, has been untreatable. Recent innovations in drug therapies have made it highly desirable to obtain sensitive biomarkers of disease progression that can be used to quantify the performance of candidate disease modifying drugs. MRI allows visualisation of bone erosion, bone marrow oedema and synovial inflammation, which are important features in RA [1]. Longitudinal imaging using MRI has been proposed as an effective tool for clinical studies, but analysis is based on visual inspection or interactive analysis [2]. We applied image registration and analysis algorithms to automatically quantify local changes in the talus bone in *in-vivo* serial MR images of an ankle in a rat model of RA by measuring bone lesion volume.

Materials and methods:

Data was obtained from 11 Lewis rats. Animals were housed, maintained, and experiments conducted, in accordance with the Home Office Animals (Scientific Procedures) Act 1986, UK. RA-like responses were induced by 2 injections of proteoglycan polysaccharide (PG-PS) from Streptococcus pyogenes at Day –14 (intra-articular) and Day 0 (systemic) [3]. The right ankle was scanned at Days -12, -4, +3, +10, +14 and +21. The T1-weighted images were acquired on a 7T 20cm bore Bruker Biospec™ and a Birdcage coil using a 3D gradient echo sequence with the following parameters: TE = 3ms, TR = 14ms, flip angle = 30°, FOV = 15×40×15mm^3, matrix = 256×256×256, corresponding to a voxel size of 58.6×156×58.6 μm.

Analysis was performed using an algorithm which automatically identifies candidate bone lesion regions in the talus bone. The approach is based on two observations: firstly that lesions appear "bright" in registered differences images, secondly that the location of lesions is consistent across subjects. The *difference images* were generated by rigid registration [4] of the talus bones in baseline and follow-up images of all the subjects, followed by subtraction (follow-up image minus baseline image). The talus bones in the *baseline images* of all subjects were mapped to a *common image space* (i.e. to a reference image) using nonrigid registration [5;6]. Otsu's thresholding technique [7] was applied to the difference images to identify bright voxels that were potential sites of pathology. Mathematical morphological operators were used to remove isolated bright voxels, and the remaining bright voxels in all the time points were transformed into the common image space. The results for all subjects were then summed to generate candidate bone lesion regions in the common image space. Connected component analysis was used to identify distinct lesion regions. The bone lesion volume in each candidate bone lesion region was calculated after mapping the regions back to the original image coordinates of each subject at each time point, enabling the lesion volume at each time point for each subject to be automatically determined. ANOVA and t-tests (with Bonferroni correction) were used for statistical analysis to compare lesion volume in each candidate lesion region in male and female subjects, and between time points.

Results:

Eight candidate bone lesion regions were automatically identified in the talus bones of this cohort of 11 subjects, as shown in the rendering in Figure 1. The average bone lesion volume of male (n=6) and female (n=5) rats in region 4 is shown in Figure 2. The gender difference in this region was significant ($p < 0.024$). Gender differences were also seen in regions 1 and 5. Significant changes between some time points were also detected in the same regions. In an initial histology assessment (one animal, single slice) at the final time point, bone erosions were confirmed in two of the regions identified by MRI as being at risk.

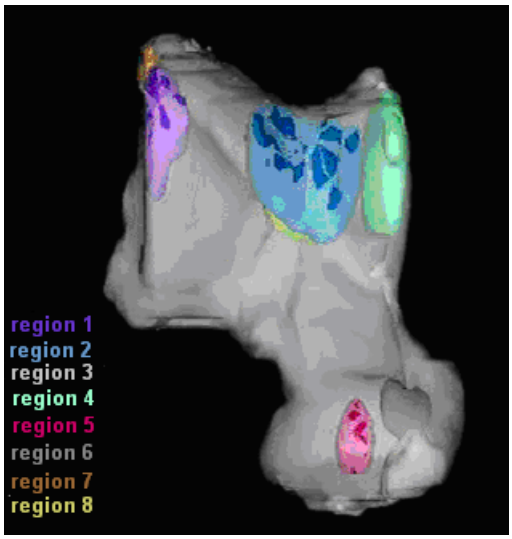

Figure 1 surface rendering of candidate bone lesion regions overlaid with the semi-transparent talus bone in the atlas. Each candidate bone lesion region is presented in a different colour as specified by the legend on the bottom left corner.

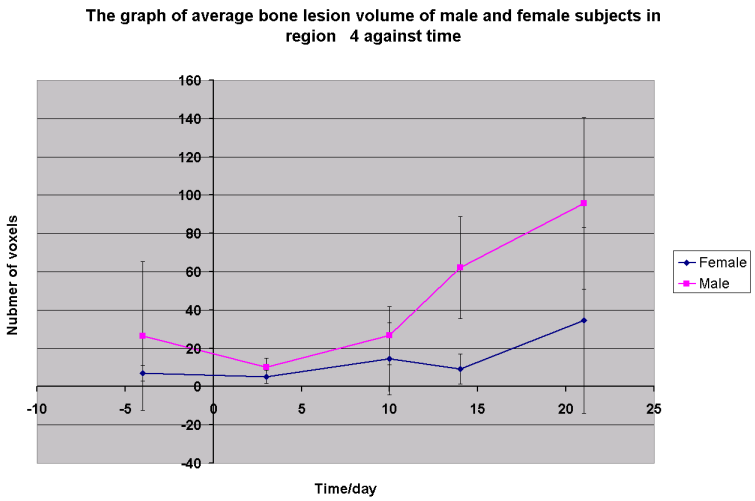

Figure 2 shows the graph of average bone lesion volume of male and female subjects in region 4 against time. Error bar in the graph shows the standard deviation of the average bone lesion volume.

Conclusions and discussions:

Automated objective methods for identifying bone lesions in longitudinal imaging studies of RA progression would be of great value in preclinical and clinical therapeutic testing. We have devised a procedure to automatically identify and quantify bone lesions in serial MR images of joints. The technique was applied to analyse the talus bones of 11 subjects that were scanned at 6 time points each. A total of eight regions at risk of lesion development were identified and portrayed using surface rendering to allow 3D visualisation. In each region at risk, lesion volumes can be quantified and plotted against time to show the progression of bone damage.

References:

1. M. Ostergaard and M. Szkudlarek, Scandinavian Journal of Rheumatology, vol. 32, no. 2, pp. 63-73, 2003.
2. F. McQueen *et al*, J Rheumatol., vol. 30, no. 6, pp. 1387-1392, June2003.
3. R. E. Esser *et al*, *Arthritis Rheum.*, vol. 28, no. 12, pp. 1402-1411, Dec.1985.
4. D. L. Hill *et al*, Physics in Medicine & Biology., vol. 46, no. 3, pp. R1-45, Mar.2001.
5. D. Rueckert *el al*, Medical Imaging, IEEE Transactions on, vol. 18, no. 8, pp. 712-721, 1999.
6. M. Holden *et al*, IEEE Trans. Med Imaging, vol. 21, no. 10, pp. 1292-1301, Oct.2002.
7. N. Otsu, IEEE Transactions on Systems, Man, and Cybernetics, vol. 9, no. 1, pp. 62-66, 1979.